Absorption Mode FTICR Mass Spectrometry Imaging

Donald F. Smith,[†,§] David P. A. Kilgour,[*,‡,§] Marco Konijnenburg,[†] Peter B. O'Connor,[‡] and Ron M. A. Heeren[*,†]

[†]FOM Institute AMOLF, Science Park 104, Amsterdam, North Holland, 1098 XG The Netherlands

[‡]Department of Chemistry, University of Warwick, Coventry, CV4 7AL United Kingdom

ABSTRACT: Fourier transform ion cyclotron resonance mass spectrometry offers the highest mass resolving power for molecular imaging experiments. This high mass resolving power ensures that closely spaced peaks at the same nominal mass are resolved for proper image generation. Typically higher magnetic fields are used to increase mass resolving power. However, a gain in mass resolving power can also be realized by phase correction of the data for absorption mode display. In addition to mass resolving power, absorption mode offers higher mass accuracy and signal-to-noise ratio over the conventional magnitude mode. Here, we present the first use of absorption mode for Fourier transform ion cyclotron resonance mass spectrometry imaging. The Autophaser algorithm is used to phase correct each spectrum (pixel) in the image, and then, these parameters are used by the Chameleon work-flow based data processing software to generate absorption mode "Datacubes" for image and spectral viewing. Absorption mode reveals new mass and spatial features that are not resolved in magnitude mode and results in improved selected ion image contrast.

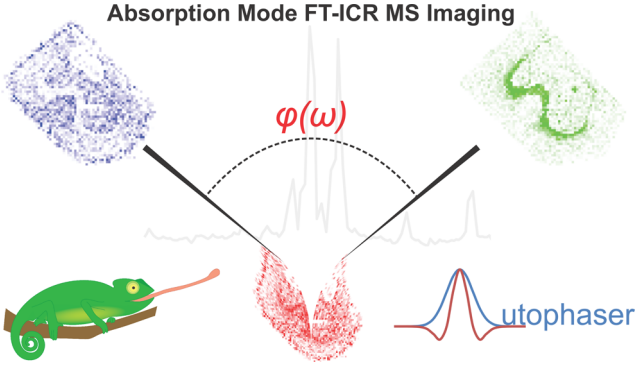

Mass spectrometry imaging (MSI) allows for the sensitive spatial mapping of biomolecules directly from complex surfaces, such as thin tissue sections.[1] Much work has been done on improving the spatial resolution of such experiments by reducing the probe size. Now, spatial resolution for MALDI MSI is typically in the range of 10−100 μm for commercial imaging mass spectrometers. Thus, improvement of the mass resolution has started to see increased attention. With such complex biomolecular surfaces, it can be expected that there will be hundreds if not thousands of individual species on the surface, yielding complex mass spectra with many ions per nominal mass that must be resolved. Fourier transform mass spectrometers, such as Fourier transform ion cyclotron resonance[2] (FTICR) and orbital trapping[3,4] (the Thermo Fisher orbitrap) are now being used routinely for MALDI MSI at mass resolving power ($m/\Delta m_{50\%}$) easily above 30 000.[5−8] Such high mass resolving power reveals spectral and thus spatial features that cannot be distinguished on lower performance mass spectrometers.

However, most FT-MS instruments have additional, unrealized performance that can be employed for MSI experiments, with no necessary hardware improvements. This lies in the way the mass spectra are presented. The two principal methods of displaying FTICR MS data are magnitude mode and absorption mode. Absorption mode spectra, which are derived from the same original transient, offer improved mass resolving power, signal-to-noise ratio and mass accuracy over magnitude mode spectra.[9−16] Magnitude and absorption mode spectra differ by the way they plot the complex output of the Fourier transformation of the transient signal. A complex number can be expressed as $a + bi$. Magnitude mode spectra are presented by plotting the length of the complex vector, for each point, versus frequency; the length of the complex vector is calculated as shown in eq 1.

$$\sqrt{(a^2 + b^2)} \tag{1}$$

In absorption mode spectra, the real part, a, of the complex number could be plotted versus frequency if all ions in the ion cloud had the same initial phase angle when the collection of the transient signal began. However, in the normal modes of operation of an FTICR MS instrument, the ions are excited by an excitation waveform; commonly, a linear frequency sweep (chirp),[17] stepped ramp, or stored waveform inverse Fourier transform signal (SWIFT).[18] All of these excitation waveforms result in the ion clouds of different m/z ions starting with different phase angles, relative to the cell detection plates, where these phase angles vary quadratically as a function of the measured ion oscillation frequency. For example, a linear frequency sweep excitation has been shown to result in the initial phase angle of ions varying quadratically as a function of measured ion frequency as shown in eq 2.[16]

$$\varphi_x = \frac{-\omega_x^2}{2R} + \omega_x\left(\frac{\omega_{Final}}{R} - \frac{2\Delta\omega_K}{2R} + t_{Delay}\right) + \left(\frac{-\omega_0^2}{2R} + \varphi_i\right) + \frac{\Delta\omega_K\omega_{Final}}{R} \quad (2)$$

Here, φ_x is the phase angle (rad) of an ion detected with an oscillation frequency ω_x (rad/s) at the start of the detection period of the ion transient, R is the ramp rate of the frequency sweep (rad/s^2), ω_0 and ω_{Final} (both rad/s) are the initial and final frequencies in the frequency sweep, respectively, $\Delta\omega_K$ (rad/s) is the mean change in frequency exhibited by an ion during excitation as a result of electrical field imperfections that may be due to the cell design or space charge related effects, t_{Delay} is the delay time between the end of the excitation waveform application and the start of the detection period, and φ_i (rad) is the initial phase of the excitation waveform.

Normally, the value of the $\Delta\omega_K$ cannot be determined ab initio, so even if the information on the frequency range and ramp rate of the excitation waveform and the delay time after excitation and before detection is known, it may be necessary to optimize the phase correction function (eq 2) to allow for variation in $\Delta\omega_K$. This optimization can be achieved using either an iterative or genetic algorithm based approach, and both have been shown to be successful.[16,19] Even if the excitation and delay parameters for a particular spectrum are not known, information within the spectrum can be used to derive the phase correction function (including the $\Delta\omega_K$ effect) using manual or automated approaches.[15,16,20] A third option for the production of a phase correction function for a particular spectrum is to use the optimized phase correction function for a similar spectrum and then optimize this curve (which should already be a good estimate) to the data in the new spectrum. Phase correction parameters will differ as a result of changes to the $\Delta\omega_K$ value, which result from variations in the space charge conditions (number of ions) from spectrum to spectrum. This optimization can also be achieved by the same iterative or genetic algorithm based approaches. Once the relationship between frequency and initial phase has been determined for a given spectrum, the phase corrected absorption mode spectrum can be plotted, both of which have been described in detail previously.[14−16]

The use of absorption mode for FTICR MS imaging experiments offers a number of advantages. First, an increase in mass resolving power, without instrumental modifications, is possible. This allows features that are not resolved in magnitude mode to be revealed in absorption mode. Also, at a given mass resolving power, experiments in absorption mode can be completed in approximately half the time of those in magnitude mode. That is, for a time domain transient of size "L", an absorption mode transient of size "$L/2$" will yield approximately the same mass resolving power of a full length transient in magnitude mode of size "L". This also reduces the size of the raw data collected, which is important when large sample sets are being measured (e.g., for clinical samples), for large area imaging or for high spatial resolution images. Further, a signal-to-noise ratio (S/N) improvement is expected,[15] which should improve selected ion images of lower abundance peaks, as well as improve the image contrast for most ion images.

Here, we describe the first use of absorption mode spectra for FTICR MS imaging. Phasing parameters for absorption mode are calculated for every spectrum (pixel) of an MS imaging run in Autophaser 6.1;[16] mass spectra are subsequently phased in the Chameleon data processing software, and high mass resolution "Mosaic Datacubes" are created.[7] Absorption mode yields superior mass resolving power and mass accuracy over magnitude mode.

EXPERIMENTAL SECTION

A mouse brain coronal section (female type 9 CFW-1, Harlan, Boxmeer, The Netherlands) was prepared on a cryo-microtome (Microm International, Walldorf, Germany) and thaw mounted to an indium-tin-oxide coated glass slide (ITO; 4−8 ′Ω resistance, Delta Technologies, Stillwater, MN, USA). The sample was coated with a 20 mg/mL solution of 2,5-dihydroxybenzoic acid (DHB; 1:1 methanol/water (0.2% trifluoroacetic acid)) with a Bruker ImagePrep. Positive-ion mode MALDI spectra were collected with a Bruker solariX FTICR MS (Bruker Daltonics, Billerica, MA, USA) equipped with a 9.4 T superconducting magnet. The laser was operated at 1 kHz, and 200 laser shots were collected at a stage raster size of 200 μm. Time domain transients of 2 mega-points (32 bit integer) were collected for a magnitude-mode Fourier limited mass resolving power of 180 000 at m/z 700.

Autophaser v6.1 was used to automatically phase correct every spectrum of the MS imaging run. This new functionality in Autophaser can read Bruker and AMOLF AWG (arbitrary waveform generator)[21] FTICR MS imaging data sets and saves the phasing parameters for each spectrum (pixel) in the imaging experiment to a text file. First, the phase correction parameters of a representative spectrum (i.e., a single pixel) are optimized. The phase correction function for this pixel is then used as a starting point for optimization for every other spectrum (pixel) in the imaging run. This method is faster than generating a new phase correction function for each pixel individually (saving ∼100−500 ms per spectrum), which is possible but would greatly slow down the data processing rate. After phase correction in Autophaser, the AMOLF developed Chameleon software was used for data processing,[7] where Mosaic Datacubes of 0.75 mDa were created and threshold peak picking was performed (threshold corresponding to a signal-to-noise ratio (S/N) of 5 at m/z 700). For magnitude mode, transients were apodized with an exponential function and zero-filled twice before fast Fourier transform (FFTW[22]), mass calibration, and insertion into the Mosaic Datacube. For absorption mode, Chameleon reads the phasing parameters generated from Autophaser and phase corrects each spectrum after Fourier transformation and before further processing. Two zero fills were used for absorption mode, with no apodization function. Two zero fills were used in order to provide sufficient points for spectral binning in the high mass resolution Mosaic Datacube. Selected ion images (selection width of ±0.001 Da) and summed mass spectra were exported from the AMOLF Datacube Explorer software. Peaklists were analyzed with in-house developed Matlab code (MATLAB version 7.13.0.564 (64 bit), Mathworks, Natick, USA) for comparison of mass resolving power, mass accuracy, and signal-to-noise ratio. For comparison of these performance metrics, no additional processing was done before the Fourier transformation (i.e., no zero-filling or apodization). Lipids were identified by comparison to the LIPID MAPS database (LIPIDMetabolites and Pathways Strategy; http://www.lipidmaps.org) using a mass tolerance of ±0.005 Da.

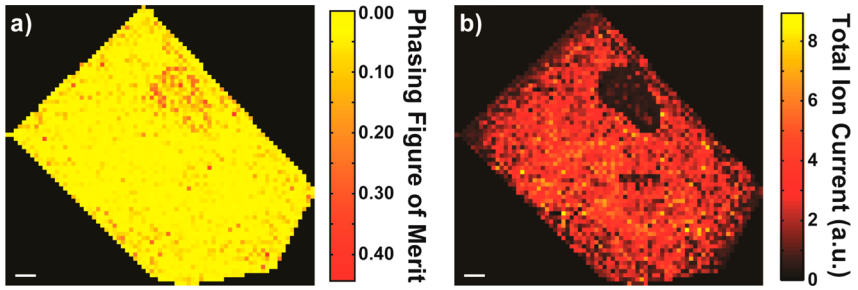

Figure 1. (a) Phasing figure of merit plotted per pixel and (b) total ion current image. The dark spot on the top right of the total ion current image is from the spotting of an oligosaccharide standard on the tissue. This results in a low number of ions and thus adversely affects the quality of the spectral phasing, as demonstrated with the higher $FoM_{PixelConfidence}$ values in this region. Scale bar = 1 mm.

Table 1. Performance Metrics for Absorption Mode versus Magnitude Mode for a MALDI FTICR MS Imaging Experiment of a Mouse Brain Section[a]

		absorption mode		magnitude mode			
mass	designation	average $m/\Delta m_{50\%}$	RMS error	average $m/\Delta m_{50\%}$	RMS error	improvement $m/\Delta m_{50\%}$	improvement RMS error
734.5694	PC(32:0) H^+	299 722	0.86	182 282	1.79	1.64	2.08
760.5851	PC(34:1) H^+	292 272	0.83	193 722	1.30	1.51	1.57
772.5253	PC(32:0) K^+	285 123	0.68	195 130	1.78	1.46	2.62
798.5410	PC(34:1) K^+	250 074	1.53	147 856	1.98	1.69	1.29
848.5566	PC(38:4) K^+	228 061	0.33	198 960	0.48	1.14	1.45

[a]Root-mean-square error is in parts-per-million.

RESULTS AND DISCUSSION

Autophaser estimates the confidence one can place in the quality of the spectral phasing for each pixel, and this information is stored in the same text file where the phase correction parameters are saved, as the figure of merit ($FoM_{PixelConfidence}$).[16] This $FoM_{PixelConfidence}$ is the RMS of the sine of the residual phase angle (after phase correction) for all detected peaks in the absorption mode spectrum. Therefore, on a perfectly phase corrected, noise free spectrum, this $FoM_{PixelConfidence}$ would be zero and a poorly phase corrected spectrum would have a large error. Very sparse spectra, or spectra containing only a small number of peaks which are significantly above the signal-to-noise floor, may be difficult to phase correct accurately because there are only a small number of peaks from which to calculate the phase correction function. This circumstance can be identified because of the anomalous $FoM_{PixelConfidence}$ values that will be returned for these pixels, relative to $FoM_{PixelConfidence}$ values of other pixels from the same image. Smaller phase correction errors can result because the phase value at the top of the peak must be interpolated because there will be a finite number of points across the peak. Therefore, for low S/N peaks, the influence of noise can introduce a small, random, phase error onto the recorded phase value interpolated at the peak top and this will be detected by this method. For low signal-to-noise spectra, these errors on the peaks, which are also being used to optimize the phase correction function, could have adversely affected the accuracy of the optimized phase correction function. Thus, anomalously high $FoM_{PixelConfidence}$ values can be used to direct the attention of the analyst to pixels which may not have been correctly phase corrected, in order to allow the severity or cause of any mis-phasing to be investigated. Figure 1a shows the $FoM_{PixelConfidence}$ plotted per pixel in an image format. In general, the relatively dense lipid spectra from positive-ion mode MALDI on tissue results in high quality phase correction functions. These dense spectra yield good absorption mode spectra, as indicated by the low $FoM_{PixelConfidence}$ values that imply Autophaser identified these pixels as phased correctly with a high confidence. However, in the area in the top right of the tissue section, the confidence has diminished. As shown in Figure 1b, the total ion current for pixels in this area is low, due to a small amount of oligosaccharide standard that was spotted on top of the tissue section (after matrix deposition). This deposition has washed many of the lipids out of this spot which results in low ion yields. Thus, the sparse spectra are more difficult to phase correctly and the quality of the phasing is reduced. As with mass calibration, phase correction of FTICR MS spectra can only be reliably undertaken on spectra that contain a sufficient number of peaks which exhibit intensities which are statistically significant above the S/N floor. Further, similar to mass calibration,[7,8] the phasing parameters are dependent on abundance fluctuations. Thus, each spectrum (pixel) must be phased individually for optimum results.

Spectral performance metrics for absorption mode versus magnitude mode are shown in Table 1 for several common phosphatidylcholine lipids (PC). The improvement in mass resolving power ($m/\Delta m_{50\%}$) is as expected; a 1.1−1.7 -fold improvement from absorption over magnitude mode. This has two major implications for FTICR MS imaging applications. First, previously collected MS imaging runs can be reprocessed with higher mass resolving power than that used previously to improve data quality. Second, the same level of mass resolving power, as collected in magnitude mode, can now be achieved in absorption mode in half of the time (collection of a time domain transient of half the size of magnitude mode). This is highly advantageous due to the relatively low repetition rate of FTICR as compared to other imaging mass spectrometers. Further, this reduction in time domain transient size also reduces the size of the raw data collected, which helps to ease data volume concerns with FTICR MS imaging. Improvements in root-mean-square (RMS) error range from 1.3−2.6 -fold for absorption versus magnitude mode, which indicate that the

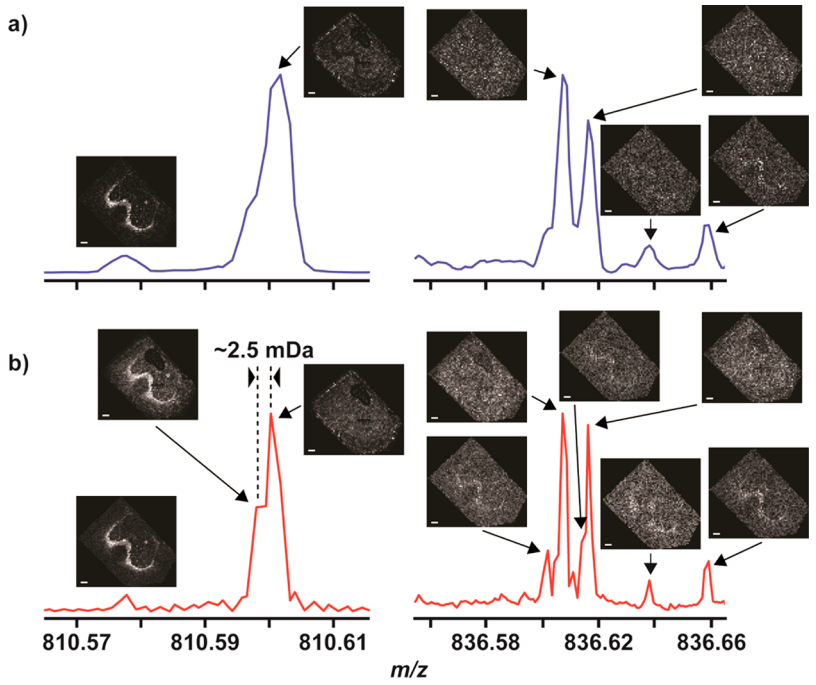

Figure 2. Summed mass spectra and selected ion images from 0.00075 Da bin Mosaic Datacubes for (a) magnitude mode and (b) absorption mode. Absorption mode yields improved line shapes and increased image contrast and uncovers features not resolved in magnitude mode. Scale bar = 1 mm and image selection width is ±0.001 Da. Spectra have been scaled to the highest peak in the spectral window.

peak center is more accurately represented in the absorption mode. The S/N improvement is usually 1.4× in absorption mode over magnitude mode, due to the discarding of the noise from the imaginary dimension. For MS imaging, this means low abundance peaks are more readily observed and selected ion images should show improved contrast. Here, we see a relative improvement in signal intensity for absorption mode versus magnitude mode. We are currently working to implement a baseline correction algorithm into Chameleon (as discussed below) for a quantitative evaluation of the S/N improvement.

Figure 2 shows a comparison between magnitude mode (Figure 2a) and absorption mode (Figure 2b) summed mass spectra at 0.75 mDa bin size. The zoom spectra clearly show the improvement in spectral line shape expected for absorption mode. Also visible in the absorption mode spectra are distortions in the baseline near the signal peaks;[23] implementation of a baseline correction algorithm in Chameleon to correct for these distortions is underway (this correction can already be made for individual spectra in Autophaser). The selected ion images for magnitude versus absorption mode are similar; however, absorption mode displays slightly higher image contrast, as expected with the improved S/N. The zoom spectra at m/z 810, shown on the left of Figure 2, demonstrate the advantage of the improved mass resolving power in absorption mode. In magnitude mode, the peak at m/z 810.6 appears to be a single peak with a large shoulder on the left side. However, in absorption mode, the shoulder of the peak reveals itself as a distinct spectral feature that is ~2.5 mDa (0.0025 Da) less than the higher abundance peak. The selected ion image of this feature shows that it has a completely different spatial distribution than the higher abundance peak, where the lower mass peak is distributed in the corpus callosum but the higher mass peak is more homogeneously distributed. An exact mass database search identifies these two lipids as PC 36:1 (810.5983; $[M + Na]^+$) and PC 38:4 (810.6007; $[M + H]^+$). Even at a mass spectral bin size of 0.75 mDa, these two peaks cannot be resolved in the magnitude mode. These peaks have a mass difference of 0.0024 Da, so with equal abundance, a mass resolving power of 337 750 is required to resolve these two peaks (at half height), which is above the Fourier limit in magnitude mode for the experimental parameters used here.

The zoomed spectra on the right of Figure 2, at m/z 836, again show the improved mass resolving power in absorption mode that allows new spectral features to be identified which are not resolved in the magnitude mode summed spectrum. In the magnitude mode, most of the peaks in this range do not show good selected ion images. However, in absorption mode, the images show tissue specific features, which include the corpus callosum and more evenly distributed ions which show the area where the standard was spotted on the tissue. Figure 2 exemplifies the advantage of higher mass resolving power for FTICR MS imaging by the use of absorption mode, mainly, improved mass resolving power to allow very closely spaced peaks (here, ~2.5 mDa) to be resolved across an entire tissue section and with increased S/N. Figure 2 also indicates the high complexity of biological tissue sections and the need for high mass resolving power to ensure resolution of tissue related ions and proper image generation.

■ CONCLUSIONS

The use of absorption mode spectra for FTICR MS imaging results in improved mass resolving power and mass accuracy. The increased mass resolving power reveals features that are unresolved in magnitude mode. Additionally, improved signal-to-noise ratio results in better image contrast. The current pipeline supports previously collected FTICR MS imaging data, so that old data sets can be reanalyzed with superior mass resolving power. Further, the method can be used to decrease the measurement time of FTICR MS imaging experiment by approximately a factor of 2, while maintaining nearly the same

mass resolving power that would have been achievable in the conventional magnitude mode (which would require a time domain transient of twice the length). Autophaser is available free for academic use, and Chameleon is available upon request.[24]

Importantly, the results described here suggest that, even at mass resolving power >250 000, there remain unresolved features from MALDI analysis of thin tissue sections, which indicates even higher mass resolving power is needed for proper image generation and interpretation. Future work will focus on phase correction within the Chameleon processing workflow to allow phasing and Datacube generation in a single processing step and the addition of a proper baseline correction algorithm to remove distortions near signal peaks.

AUTHOR INFORMATION

Corresponding Authors

*E-mail: d.p.a.kilgour@warwick.ac.uk (D.P.A.K.).

*E-mail: heeren@amolf.nl (R.M.A.H.).

Author Contributions

[§]D.F.S. and D.P.A.K. contributed equally.

Notes

The authors declare no competing financial interest.

ACKNOWLEDGMENTS

This work is part of the research program of the Foundation for Fundamental Research on Matter (FOM), which is part of The Netherlands Organisation for Scientific Research (NWO). This publication was supported by the Dutch national BSIK program COMMIT. The authors thank the EPSRC: Warwick Centre for Analytical Sciences (EPSRC: P/F034210/1) and the Department of Chemistry, University of Warwick for funding. Portions of this research were supported by the American Reinvestment and Recovery Act of 2009 and the U.S. Department of Energy (DOE) Office of Biological and Environmental Research. Portions of the research described in this article were performed at the W. R. Wiley Environmental Molecular Sciences Laboratory, a national scientific user facility sponsored by the Department of Energy's Office of Biological and Environmental Research and located at Pacific Northwest National Laboratory (PNNL). PNNL is operated by Battelle for the U.S. Department of Energy under Contract DE-AC05-76RLO 1830.

REFERENCES

(1) Chughtai, K.; Heeren, R. M. A. *Chem. Rev.* **2010**, *110*, 3237−3277.

(2) Marshall, A. G.; Hendrickson, C. L.; Jackson, G. S. *Mass Spectrom. Rev.* **1998**, *17*, 1−35.

(3) Makarov, A. *Anal. Chem.* **2000**, *72*, 1156−1162.

(4) Zubarev, R. A.; Makarov, A. *Anal. Chem.* **2013**, *85*, 5288−5296.

(5) Cornett, D. S.; Frappier, S. L.; Caprioli, R. M. *Anal. Chem.* **2008**, *80*, 5648−5653.

(6) Rompp, A.; Guenther, S.; Takats, Z.; Spengler, B. *Anal. Bioanal. Chem.* **2011**, *401*, 65−73.

(7) Smith, D. F.; Kharchenko, A.; Konijnenburg, M.; Klinkert, I.; Pasa-Tolic, L.; Heeren, R. M. A. *J. Am. Soc. Mass Spectrom.* **2012**, *23*, 1865−1872.

(8) Barry, J. A.; Robichaud, G.; Muddiman, D. C. *J. Am. Soc. Mass Spectrom.* **2013**, *24*, 1137−1145.

(9) Marshall, A. G. *J. Chem. Phys.* **1971**, *55*, 1343.

(10) Comisarow, M. B. *J. Chem. Phys.* **1971**, *55*, 205.

(11) Comisarow, M. B.; Marshall, A. G. *Can. J. Chem.* **1974**, *52*, 1997−1999.

(12) Marshall, A. G.; Roe, D. C. *Anal. Chem.* **1978**, *50*, 756−763.

(13) Marshall, A. G.; Verdun, F. R. *Fourier Transforms in NMR, Optical, and Mass Spectrometry: A User's Handbook*; Elsevier Science and Technology, Elsevier Science Ltd: Oxford, UK, 1990.

(14) Xian, F.; Hendrickson, C. L.; Blakney, G. T.; Beu, S. C.; Marshall, A. G. *Anal. Chem.* **2010**, *82*, 8807−8812.

(15) Qi, Y.; Barrow, M. P.; Li, H.; Meier, J. E.; Van Orden, S. L.; Thompson, C. J.; O'Connor, P. B. *Anal. Chem.* **2012**, *84*, 2923−2929.

(16) Kilgour, D. P. A.; Wills, R.; Qi, Y.; O'Connor, P. B. *Anal. Chem.* **2013**, *85*, 3903−3911.

(17) Comisarow, M. B.; Marshall, A. G. *Chem. Phys. Lett.* **1974**, *26*, 489−490.

(18) Guan, S. H.; Marshall, A. G. *Int. J. Mass Spectrom. Ion Process* **1996**, *157*, 5−37.

(19) Kilgour, D. P. A.; Neal, M. J.; Soulby, A. J.; O'Connor, P. B. *Rapid Commun. Mass Spectrom.* **2013**, *27*, 1977−1982.

(20) Qi, Y.; Thompson, C.; Van Orden, S.; O'Connor, P. *J. Am. Soc. Mass Spectrom.* **2011**, *22*, 138−147.

(21) Mize, T. H.; Taban, I.; Duursma, M.; Seynen, M.; Konijnenburg, M.; Vijftigschild, A.; Doornik, C. V.; Rooij, G. V.; Heeren, R. M. A. *Int. J. Mass Spectrom. Ion Process* **2004**, *235*, 243−253.

(22) Frigo, M.; Johnson, S. G. *Proc. IEEE* **2005**, *93*, 216−231.

(23) Xian, F.; Corilo, Y. E.; Hendrickson, C. L.; Marshall, A. G. *Int. J. Mass Spectrom. Ion Process* **2012**, *325*, 67−72.

(24) Autophaser: www.warwick.ac.uk/autophaser. For Chameleon, contact m.konijnenburg@amolf.nl (M.K.) or heeren@amolf.nl (R.M.A.H.).